

DESIGN AND OPTIMIZATION OF VARIABLE STIFFNESS 3D PRINTING CFRP COMPOSITES PYRAMID LATTICE SANDWICH ESR PROSTHESIS FOOT

M. J. Jiang and J. X. Zhang¹

UDC 539.4

In this paper, we propose an energy return optimization method for lightweight sandwich structure composite prostheses and study the performance of 3D-printed short fiber-reinforced composites in ESR prostheses. A commercial product is used as the original model, and a lightweight pyramid lattice sandwich structure is used to design the prosthesis. A gradient optimization method is designed to optimize the forefoot, hindfoot, and midfoot energy storage characteristics for multiple working cases based on the response surface approach. The response model of the pyramid lattice sandwich structure parameters and the energy return of the prosthesis was established. The designed variable stiffness pyramid lattice sandwich structure prosthesis has a higher energy storage efficiency in heel strike (17.55%), mid-stand (20.16%), and push-off conditions (55.93%), which is more adaptable to the prosthetic walking requirements. The research method of this paper successfully realized the application of composite lightweight dot matrix sandwich structures in prostheses, and the proposed optimization method has guiding significance for the optimization of prosthetic energy returns.

Keywords: biometric prosthetic foot, energy store and return character, carbon fiber epoxy composites, pyramid lattice sandwich.

Introduction. Lower limb amputees have reached 37 million [1], with low-income people accounting for 70–80% of the population [2]. Amputees in low- and middle-income countries often use passive prosthetic feet, such as solid ankle cushion heel (SACH) prostheses, which cost only a few tens of dollars [3]. However, energy storage and return (ESR) prostheses have been shown to provide increased benefits and walking performance compared to traditional SACH feet [4]. ESR prostheses usually cost thousands of US dollars compared to tens of dollars for SACH feet, making them less accessible [5]. Creating a low-cost, mass-manufacturable ESR prosthetic foot enables the ability to perform daily activities [6].

Carbon fiber-reinforced three-dimensionally printed prosthetic feet have the potential to serve as a low-cost alternative to ESR prosthetic feet, and three-dimensional printing can function as a viable fabrication method for patient end-use prosthetic components [7]. Previous work has explored the use of sandwich structures to apply low-cost additive materials in foot and ankle prostheses [8]. Previous authors have conducted preliminary explorations to provide toe stiffness using sandwich structures. The toe joint was implemented as a single part suitable for 3D printing [9]. Stiffness is closely related to energy storage properties [10], and the pyramid lattice sandwich structure is lightweight and highly stiff [11]. Based on previous work, the sandwich structure will be used for prosthetic energy storage design.

The energy storage properties of prostheses have been studied using the following methods. The total energy stored in the prosthetic foot was calculated using trapezoidal integration of force-displacement data over the entire load range [12]. The plantar flexed foot was deformed in cyclic testing using a sinusoidal forcing function oscillating between 100 and 800 N at a frequency of 1 Hz. The energy lost during loading and unloading was measured as the area of the hysteresis loop [13]. Adamczyk et al. [14] calculated the prosthesis's energy return results using ankle

College of Mechanical Engineering, Tianjin University of Science & Technology, Tianjin, China (zjx@tust.edu.cn). Translated from Problemy Mitsnosti, No. 4, p. 123, July – August, 2023. Original article submitted February 25, 2023.

moments during amputee walking. Fey et al. [15] identified the energy expenditure using biomechanical investigation. Gait analysis is used to study various parameters of amputee walking, and several specific gait moments, such as heel strike, middle stance, and push-off, are the focus [16].

We innovatively utilized short-cut carbon fiber-reinforced composites and pioneered the application of a pyramidal lattice matrix sandwich structure in the prosthesis. We designed a variable stiffness midfoot prosthesis. By employing response surface methodology, we investigated the impact of the sandwich structure on the energy storage and return (ESR) characteristics of the prosthesis. Our goal was to design a variable stiffness pyramidal lattice matrix sandwich midfoot that offers optimal ESR characteristics for the prosthesis.

1. Materials and Methods. The prosthetic foot model was designed based on the prosthesis proposed in the literature [17], incorporating the pyramid lattice sandwich structure in the middle foot region. In this design, the lattice sandwich was implemented in the midfoot area, with the upper plate of the sandwich connected to the fixed ankle and the lower plate attached to the insole. The coupling points of the ankle joint are located identically to those in the literature prosthesis. The prosthetic foot is depicted in Fig. 1a. Except for the midfoot sandwich region, all structural parameters of the prostheses remain consistent with the literature. The midfoot fractional sandwich region is a customizable area with variable parameters such as sandwich height, plate thickness, core radius, and core angle. The designable structure parameters of the prosthetic foot are illustrated in Fig. 1b.

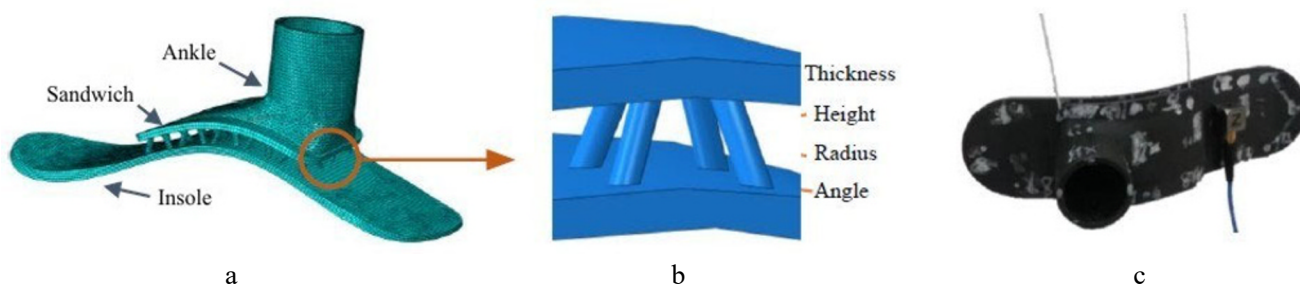


Fig. 1. (a) Pyramid lattice sandwich prosthesis foot, (b) pyramid lattice sandwich cell, and (c) dynamic frequency response test of the prosthesis sample.

Using the GB/T 13665-2007 Damping principal test method, the damping coefficient of the prosthetic structure was obtained from a dynamic experiment using the LMS SCADAS testing system, as shown in Fig. 1c). The prosthetic foot was printed using an FDM (fused deposition modeling) UltiMaker z2 3D printer (UltiMaker, Inc., Utrecht, Netherlands). Short fiber-reinforced composite ePA-CF nylon (ESUN, Inc., China) was used with a layer height of 0.1 mm. The EPA-CF is a nylon 6/66 copolymer with 20% carbon fiber added, and the material characteristics of the printed prosthesis can be found in Table 1.

TABLE 1. Mechanical Property Parameters of the EPA-CF Prosthetic Foot

| Density (g/cm ³) | Bending strength (MPa) | Bending modulus (MPa) | Damping coefficient |
|------------------------------|------------------------|-----------------------|---------------------|
| 1.24 | 140 | 4363 | 0.06 |

The FE model in ABAQUS incorporates blades meshed using solid components C3D8R. Three working cases of the ISO 16955 standard were employed to investigate the ESR characteristics of the prosthesis. As depicted in Fig. 2a, a test rig conforms to the ISO 16955 standard, comprising a loading frame simulating the leg and a rigid plate representing the ground. The load shown in Fig. 2a is applied to the top point (point A) of the loading frame. All three cases must load the prosthetic foot to the peak value and then unload in 1 s. For the heel strike and push-off cases, the peak force is 824 N, which is 1373 N for the mid-stance case.

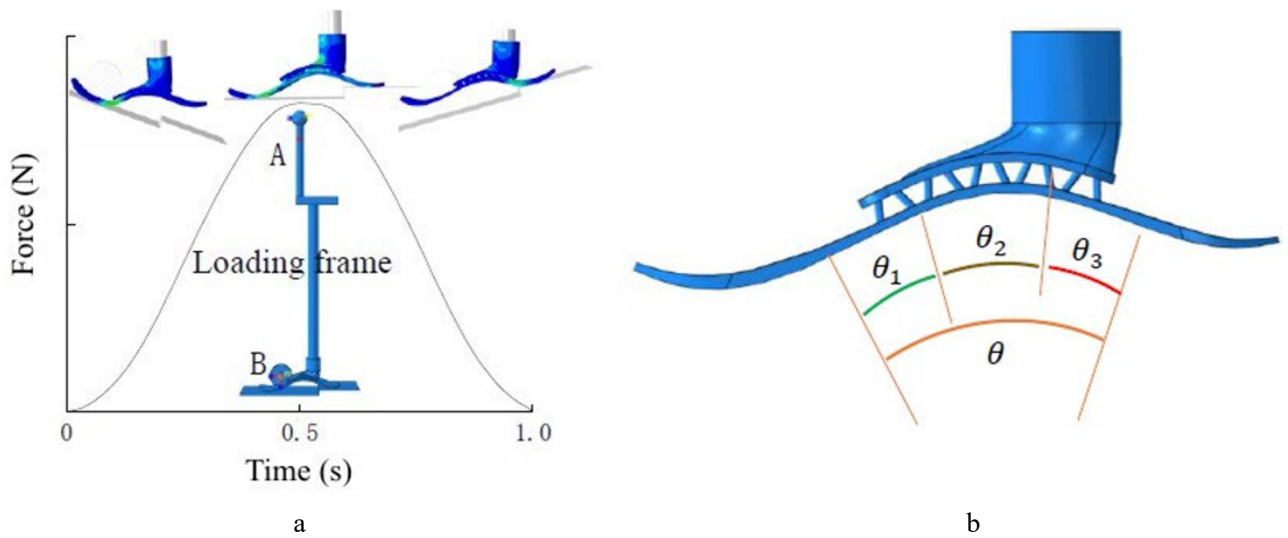


Fig. 2. Load curve, FE model, and the stress distribution of three cases (a), schematic diagram of the core region and optimized subregion (b).

By adjusting the rotation angle of the ground rigid plate around point B , the loading angles for the three conditions are achieved. In case 1, the angle between the rigid plate and the horizontal plane is -15° in case 1 (heel strike), 0° in case 2 (midstance), and 20° in case 3 (push off). Python scripts were developed to extract load-displacement data from the simulation results. Energy loss was calculated by subtracting the energy released during unloading from the energy absorbed during loading. Deformation of the heel and forefoot under a 400 N reaction force was extracted from the heel strike and push-off conditions.

The optimization is based on the comfort stiffness constraint specified in the KS P 8403 standard. According to the standard, the elastic deformation in the forefoot should range between 20 and 40 mm when subjected to a vertical force of 400 N and between 6 mm and 22 mm in the heel. The goal is to optimize the parameters of the prosthesis to satisfy these comfort stiffness requirements. The optimization problem's mathematical model is as follows:

$$\begin{cases} \text{Find } X = [x_1, x_2, \dots, x_n], \\ \min F(X) = f(x_1, x_2, \dots, x_n), \\ \text{s. t. } g_0 \leq G(X) \leq g_1. \end{cases} \quad (1)$$

The maximum stress criterion is used for the energy storage simulation. Proper parameter ranges of the independent variable were determined to prevent any damage, including the plate thickness [x_1 : (3–8 mm)], the sandwich core height [x_2 : (3–6 mm)], the core angle [x_3 : (0° – 20°)], and the core radius [x_4 : (2–6 mm)]. The dependent variables were energy loss (y_1) and displacement (y_2). The four structural parameters were optimized using the Box-Behnken design in Design-Expert 12.0 (Stat-Ease Inc., Minneapolis, MN), and a 27-run simulation was conducted to test the effects of the four structural parameters at three levels: high (+1), intermediate (0), and low (–1). Response surface methodology (RSM) was then employed to establish the functional relationship between the input variables and the output response. These coefficients can be obtained through regression analysis. The following binomial polynomial was used to fit the energy loss model:

$$Y = \alpha_0 + \sum_{i=1}^n \alpha_i X_i + \sum_{i=1}^n \alpha_{ii} X_i^2 + \sum_{i=1}^n \alpha_{ij} X_i X_j + \varepsilon, \quad (2)$$

where Y is the predicted response variable; α_0 , α_i , α_{ii} , and α_{ij} are the regression coefficients of variables for intercept, linear, quadratic, and interaction terms, respectively; X_i and X_j are independent variables ($i < j$); n is the number of research factors; and ε is the error.

The variable stiffness sandwich structure was designed in the midfoot region to optimize the energy storage efficiency of the prosthesis. Taking the deformation regions of the prosthesis corresponding to the three energy storage conditions as a reference, the midfoot was divided into three subregions for the front, middle, and rear subregions, as shown in Fig. 2b, and the optimal sandwich structure parameters for the three energy storage conditions were used to design the three subregions. The relationship between the core region and the subregion is shown in the following equation. The lengths of the subregions θ_i are used as design variables, prostheses of different combinations of subregion lengths are modeled, and ESR is simulated. The combination of lengths with minimum energy loss is taken as the variable stiffness sandwich parameter for the midfoot region:

$$\sum_{i=1}^3 \theta_i = \theta (0 \leq \theta_i < \theta). \quad (3)$$

2. Results. By applying multiple regression analysis to the simulation data, the response variable and the independent variables were related by the following second-order polynomial equation:

$$y_1 = -0.2400 - 0.0009x_1 + 0.0230x_2 + 0.0325x_3 + 0.0011x_4 + 0.0326x_1x_2 + 0.0011x_1x_3 - 0.0047x_1x_4 + 0.0091x_2x_3 + 0.0839x_2x_4 + 0.0423x_3x_4 + 0.1491x_1^2 + 0.1529x_2^2 + 0.1693x_3^2 + 0.1783x_4^2, \quad (4)$$

$$y_2 = 5.4833 - 5.1901x_1 - 0.3907x_2 - 0.0147x_3 - 0.3129x_4 + 0.4773x_1x_2 + 0.0112x_1x_3 + 0.3541x_1x_4 - 0.0052x_2x_3 - 0.0594x_2x_4 + 0.0020x_3x_4 + 2.4711x_1^2 + 0.1542x_2^2 - 0.0087x_3^2 - 0.0665x_4^2, \quad (5)$$

$$y_1 = 0.1187 + 0.0002x_1 + 0.0133x_2 - 0.0019x_3 - 0.0083x_4 + 0.0607x_1x_2 + 0.0035x_1x_3 + 0.0572x_1x_4 + 0.0277x_2x_3 - 0.0161x_2x_4 + 0.0006x_3x_4, \quad (6)$$

$$y_2 = 8.1028 - 8.4260x_1 - 0.1727x_2 - 0.0241x_3 - 0.2425x_4 + 0.1627x_1x_2 + 0.0309x_1x_3 + 0.2845x_1x_4 + 0.0143x_2x_3 - 0.0513x_2x_4 + 0.0113x_3x_4 + 4.3967x_1^2 + 0.1265x_2^2 - 0.0283x_3^2 - 0.0153x_4^2, \quad (7)$$

$$y_1 = 0.0239 - 0.0724x_1 - 0.0076x_2 - 0.0074x_3 + 0.0066x_4 + 0.0196x_1x_2 + 0.0118x_1x_3 - 0.0133x_1x_4 + 0.0005x_2x_3 - 0.0011x_2x_4 - 0.0042x_3x_4 + 0.0557x_1^2 - 0.0019x_2^2 - 0.0049x_3^2 + 0.0065x_4^2. \quad (8)$$

Equation (4) represents the energy loss for the heel strike case, Eq. (5) denotes the displacement of the heel strike case, Eq. (6) corresponds to the energy loss for the push-off case, Eq. (7) denotes the displacement of the push-off case, and Eq. (8) represents the energy loss for the mid-stance condition.

Table 2 shows the target value structure parameters.

TABLE 2. Optimization Results of Structural Parameters and Minimum Energy Loss Values

| Case | BH | CH | ANGLE | CR | Energy loss | Displacement |
|------------|-------|-------|-------|-------|-------------|--------------|
| Heel-stick | 4.284 | 4.124 | 7.028 | 3.531 | 0.083 | 6.027 |
| Push-off | 4.003 | 3.956 | 3.683 | 2.822 | 0.132 | 21.008 |
| Mid-stand | 4.058 | 4.247 | 5.817 | 2.170 | 0.124 | |

Combining the sandwich parameters obtained from the energy storage optimization for the three operating conditions in the above table and designing the variable stiffness pyramid lattice sandwich subregion length combination scheme using energy loss, a total of four combinations are discussed, using the number of pyramid lattice sandwich cores in the three subregions to indicate the length of the pyramid lattice sandwich subregion θ_i , and the energy storage characteristics of the prosthesis with a total of four pyramid lattice sandwich combinations, 404, 152, 242 and 233. Examples of combinations are shown in Fig. 3a and 3b. The energy losses corresponding to each combination under the three operating conditions are shown in Fig. 3c.

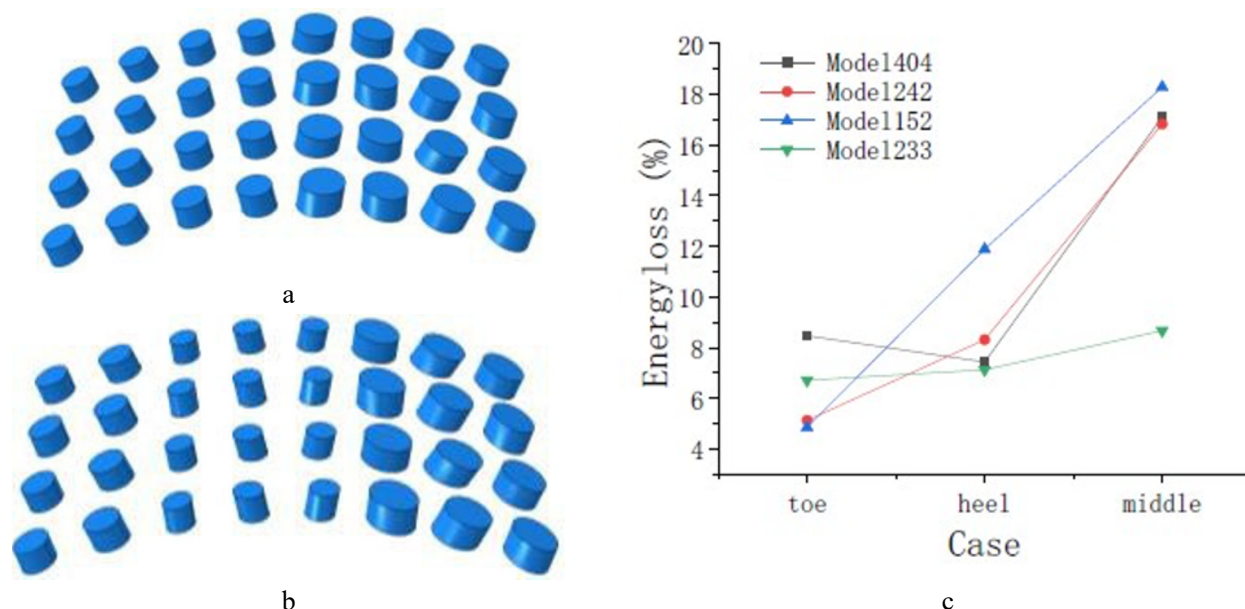


Fig. 3. Variable stiffness sandwich structure: (a) 404, (b) 233, and (c) energy loss curve.

Figure 3a shows the pyramid lattice sandwich cores for the parameters corresponding to the 4-row push-off condition in subregion θ_1 , the pyramid lattice sandwich cores corresponding to the 0-group mid-stand condition in subregion θ_2 , and the optimal pyramid lattice sandwich cores for the 4-group heel strike condition in subregion θ_3 . This combination is indicated by code 404; Fig. 3b shows the pyramid lattice sandwich core for the parameters corresponding to the 2-row push-off condition in subregion θ_1 , the θ_2 subregion 3 groups of the mid-stand working condition corresponding to the core parameters of the pyramid lattice sandwich core, and subregion θ_3 assigning three groups of the pyramid lattice sandwich core for the optimized parameters of the heel strike working condition, with 233 representing this combination of the pyramid lattice sandwich.

The simulation verifies that the 233-combination pyramid lattice sandwich has optimal energy storage characteristics and meets the comfort condition, so the 233-pyramid lattice sandwich is the optimal energy storage prosthesis solution.

3. Discussion. A prosthesis from the literature [17] was selected, modeled according to the actual parameters of the model in the literature, and attached to the composite footplate glass fiber-reinforced composite and carbon fiber woven composite properties as in the literature. The boundary conditions are the same as those in the literature using the 8403 standard. Forefoot compression and heel compression were established.

Figure 4a shows the load–displacement curve of the forefoot 30° angle bending simulation compared with the test load–displacement curve in [17], and Fig. 4b shows the simulation load–displacement curve of heel 15° angle bending compared with the test load–displacement curve in [17]. The comparison of the load–displacement curves in Fig. 4 shows that the simulation model can accurately represent the actual force situation and be used for analysis.

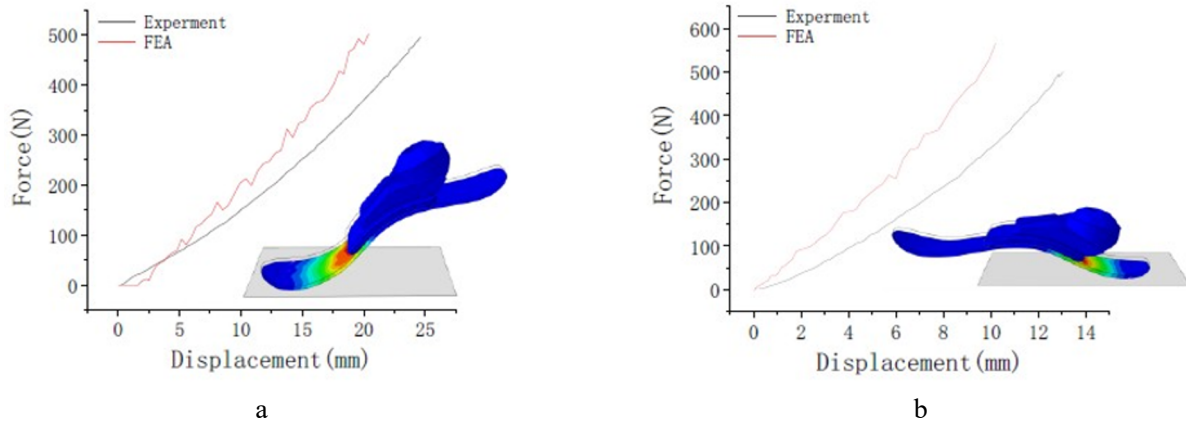


Fig. 4. Stress distribution according to the performance analysis of the modified prosthetic foot: forefoot compression load–displacement curve (a), heel compression load–displacement curve (b).

Table 3 shows the coefficient of determination P -value, the adjustment determination coefficient R^2 , and the prediction determination coefficient R^2 , indicating the model’s accuracy. The determination coefficients suggest that the fitted model of the response surface is accurate. The P -value implies that the model is significant. It can be concluded that the fitted model can be used to predict the simulation experiment.

TABLE 3. RSM Model Accuracy

| Source | Sequential P -value | Adjusted R^2 | Predicted R^2 |
|-------------|-----------------------|----------------|-----------------|
| Heel strike | 0.0005 | 0.6026 | -0.0565 |
| Heel 6–22 | < 0.0001 | 0.9983 | 0.9956 |
| Push off | 0.1902 | 0.0378 | -0.9840 |
| Fore 20–40 | < 0.0001 | 0.9991 | 0.9976 |
| Mid stance | < 0.0001 | 0.9063 | 0.7509 |

From the results of the one-factor analysis, it is clear that the heel bending fore displacement in Fig. 5a is the most sensitive to the panel thickness. Similar to the previous study, [18] discussed the effect of the panel material on the bending stiffness. The nonlinear response is the same as that obtained in the literature [19] for the displacement load of the sandwich structure.

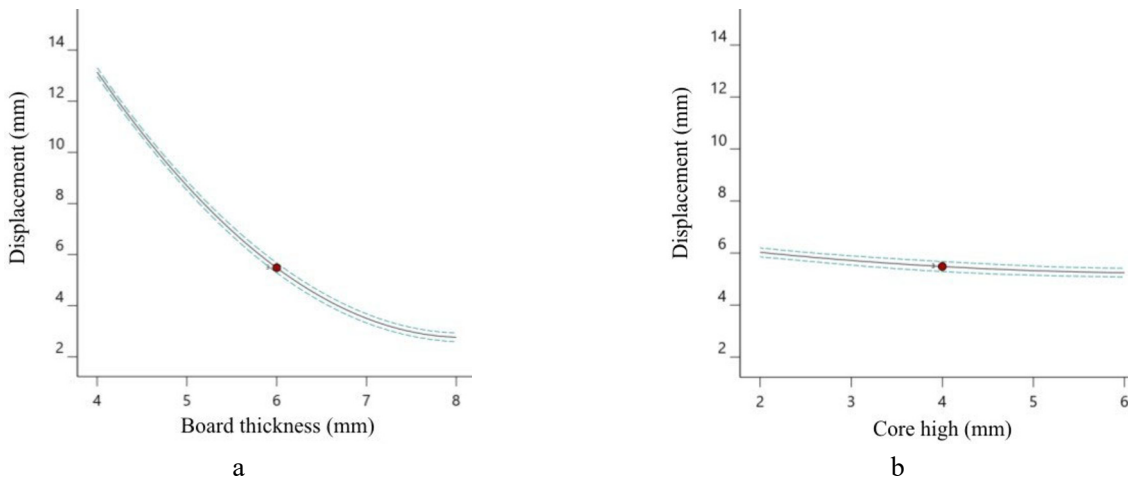


Fig. 5. One-factor analysis of the displacement 6–22 model: (a) board thickness–displacement, (b) core high–displacement.

Figure 5b shows that the stiffness increases with increasing sandwich height, i.e., the bending displacement response decreases with increasing sandwich height, which is the same as the conclusion in the literature [20]. The above discussion verifies the accuracy of the response surface model.

The energy loss was compared between the original and optimized models using the ISO 16955 standard for analyzing energy storage characteristics. The analysis encompassed three operating cases: heel strike, mid-stance, and push-off, as shown in Fig. 6.

The energy loss comparison between the original and optimized models and the corresponding energy return growth rates for the three operating cases are shown in Table 4.

TABLE 4. RSM Model Accuracy

| Case | Original model energy loss | Optimized model energy loss | Growth energy save |
|-------------|----------------------------|-----------------------------|--------------------|
| Heel strike | 0.101 | 0.083 | 17.55% |
| Mid stand | 0.155 | 0.124 | 20.16% |
| Push off | 0.299 | 0.132 | 55.93% |

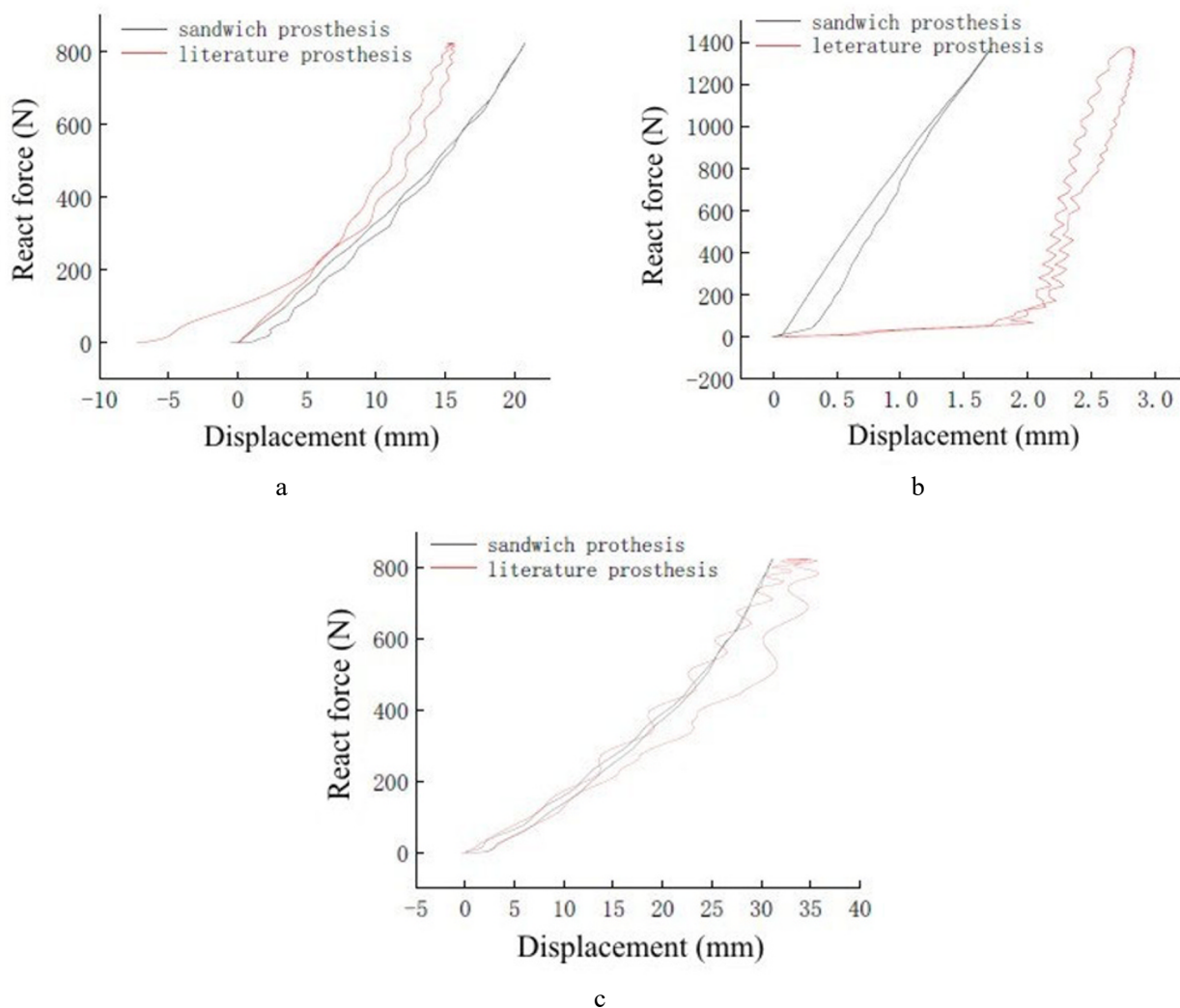


Fig. 6. Comparison of the energy storage curves of the optimized 233 model and the original model heel strike (a), mid stand (b), and push-off (c).

As shown in Table 4, the energy loss of the original model gradually increases from heel to forefoot, and the energy loss of the optimized model has the same change trend as the original model, which shows the reasonableness of the optimized model. However, the rate of energy consumption change between the optimized model's three working conditions (0.083–0.124–0.132) is lower than that of the original model (0.101–0.155–0.299). The energy storage of the optimized model increases in all three working cases compared to the original model, among which the increment of working case 3 (55.93%) is much higher than that of working case 1 (17.55%), indicating that the optimized model has obvious advantages in forefoot energy storage. In the comparison between working condition 1 and working case 3, the load values of the two conditions are equal. Still, the comfort criteria set different stiffness ranges for the forefoot and heel, and the forefoot stiffness is smaller than that of the heel, which stores more energy in the forefoot than in the heel.

Due to the limitations of the test conditions, walking tests could not be performed, and we validated the simulation model using tests from the literature.

Conclusions. This study uses short fiber-reinforced composites to apply a lightweight pyramid lattice sandwich structure in prostheses. A response surface model is established to analyze the parameters of the pyramid lattice sandwich structure, considering the energy loss and bending stiffness of the prosthesis. The impact of the sandwich structure on energy storage characteristics is examined, and multigradient optimization is conducted to achieve optimal energy storage characteristics. A variable stiffness pyramid lattice sandwich structure is designed for the forefoot, midfoot, and hindfoot, resulting in improved energy return efficiency in all three working cases. The research methodology presented in this paper demonstrates its effectiveness in designing and optimizing the energy storage characteristics of prostheses.

Acknowledgments. This research was funded by the Tianjin Postgraduate Research Innovation Project, grant number [2020YJSB065], the Tianjin Science and Technology Plan Project [20JCYBJC01430], and the Tianjin Postgraduate Research Innovation Project, grant number [2019YJSB014].

REFERENCES

1. A. Cieza, K. Causey, K. Kamenov, et al., "Global estimates of the need for rehabilitation based on the Global Burden of Disease Study 2019: a systematic analysis for the Global Burden of Disease Study 2019," *The Lancet*, **396**, No. 10267, 2006–2017 (2021).
2. C. L. McDonald, S. Westcott-McCoy, M. R. Weaver, et al., "Global prevalence of traumatic non-fatal limb amputation," *Prosthet Orthot Int*, **45**, No. 2, 105–114 (2021).
3. J. Z. Laferrier, A. Grof, S. Hale, et al., "A review of commonly used prosthetic feet for developing countries: a call for research and development," *J Nov Physiother*, **8**, No. 1, 380 (2018).
4. M. Marino, S. Pattni, M. Greenberg, et al., "Access to prosthetic devices in developing countries: pathways and challenges," in: Proc. 2015 IEEE Global Humanitarian Technology Conference (GHTC), Seattle, USA (2015), pp. 45–51.
5. E. C. Baars, E. Schrier, P. U. Dijkstra, et al., "Prosthesis satisfaction in lower limb amputees: A systematic review of associated factors and questionnaires," *Medicine*, **97**, No. 39, e12296 (2018).
6. S. Farrokhi, B. Mazzone, A. Yoder, et al., "A narrative review of the prevalence and risk factors associated with development of knee osteoarthritis after traumatic unilateral lower limb amputation," *Mil Med*, **181**, No. S4, 38–44 (2016).
7. B. J. South, N. P. Fey, G. Bosker, et al., "Manufacture of energy storage and return prosthetic feet using selective laser sintering," *J Biomech Eng*, **132**, No. 1, 015001 (2010).
8. H. H. Warder, J. K. Fairley, J. Coutts, et al., "Examining the viability of carbon fiber reinforced three-dimensionally printed prosthetic feet created by composite filament fabrication," *Prosthet Orthot Int*, **42**, No. 6, 644–651(2018).

9. H. J. Um, H. S. Kim, W. Hong, et al., "Design of 3D printable prosthetic foot to implement nonlinear stiffness behavior of human toe joint based on finite element analysis," *Sci Rep*, **11**, No. 1, 19780 (2021).
10. S. A. Ghannadpour, M. Mahmoudi, and K. H. Nedjad, "Structural behavior of 3D-printed sandwich beams with strut-based lattice core: experimental and numerical study," *Compos Struct*, **281**, 115113 (2022).
11. L. Bai, X. Yue, X. Chen, et al., "Improved mechanical properties and energy absorption of Ti6Al4V laser powder bed fusion lattice structures using curving lattice struts," *Mater Design*, **211**, 110140 (2021).
12. N. D. Womac, R. R. Neptune, and G. K. Klute, "Stiffness and energy storage characteristics of energy storage and return prosthetic feet," *Prosthet Orthot Int*, **43**, 266–275 (2019).
13. M. D. Geil, "Energy loss and stiffness properties of dynamic elastic response prosthetic feet," *J Prosthet Orthot*, **13**, 70–73(2001).
14. P. G. Adamczyk, M. Roland, and M. E. Hahn, "Sensitivity of biomechanical outcomes to independent variations of hindfoot and forefoot stiffness in foot prostheses," *Hum Movement Sci*, **54**, 154–171(2017).
15. N. P. Fey, G. K. Klute, and R. R. Neptune, "The influence of energy storage and return foot stiffness on walking mechanics and muscle activity in below-knee amputees," *Clin Biomech*, **26**, No. 10, 1025–1032 (2011).
16. P. G. Adamczyk, M. Roland, and M. E. Hahn, "Sensitivity of biomechanical outcomes to independent variations of hindfoot and forefoot stiffness in foot prostheses," *Hum Movement Sci*, **54**, 154–171 (2017).
17. Y. Song, S. Choi, S. Kim, et al., "Performance test for laminated-type prosthetic foot with composite plates," *Int J Precis Eng Man*, **20**, 1777–1786 (2019).
18. C. Bellini, R. Borrelli, F. D. Caprio, et al., "Hybrid structures in titanium-lattice/FRP: effect of skins material on bending characteristics," *Procedia Struct Integr*, **41**, 3–8 (2022).
19. S. R. Chowdhury and J. Reddy, "Geometrically exact micropolar Timoshenko beam and its application in modelling sandwich beams made of architected lattice core," *Compos Struct*, **226**, 111228 (2019).
20. C. Zeng, L. Liu, W. F. Bian, et al., "Bending performance and failure behavior of 3D printed continuous fiber reinforced composite corrugated sandwich structures with shape memory capability," *Compos Struct*, **262**, 113626 (2021).